# Interaction of a Cumulus Cloud Ensemble with the Large-Scale Environment. Part II

STEPHEN J. LORD[1] AND AKIO ARAKAWA

*Department of Atmospheric Sciences, University of California, Los Angeles 90024*

(Manuscript received 25 January 1980, in final form 1 August 1980)

ABSTRACT

The closure assumption of the Arakawa-Schubert (1974) cumulus parameterization takes the form of a balance between the generation of moist convective instability by large-scale processes and its destruction by clouds. This assumption can be justified by consideration of the kinetic energy budget of a cumulus subensemble. First, the kinetic energy generation and dissipation per unit cloud-base mass flux should approximately balance over time scales of the order of the large-scale processes. Second, the dissipation per unit cloud-base mass flux and, therefore, the kinetic energy generation per unit cloud-base mass flux (the cloud-work function) for a given subensemble should not depend substantially on the large-scale conditions. The cloud-work function quasi-equilibrium follows consequently and the unknown cloud-base mass flux is determined by an integral equation.

Observational evidence for the cloud-work function quasi-equilibrium is presented. Cloud-work functions are calculated from a variety of data sets in the tropics and subtropics including the GATE, AMTEX, VIMHEX and composited typhoon data. The results show that the cloud-work functions fall into a well-defined narrow range for each subensemble although the thermodynamical vertical structures for each data set are quite different.

## 1. Introduction

Since individual cumulus clouds are necessarily subgrid-scale in any numerical model of large-scale circulations, the collective effects of clouds within a model grid box must be expressed, or parameterized, in terms of the grid-point variables. Although it is not completely obvious that this goal may be attained, the frequent organization of the individual clouds into clusters indicates that they are statistically coupled with the large-scale dynamical and thermodynamical processes.

The first attempts to parameterize cumulus clouds were made in modeling tropical cyclones. Charney and Eliassen (1964) and Ooyama (1964) introduced the concept of Conditional Instability of the Second Kind (CISK) to describe the cooperative mechanism between cumulus-scale and cyclone-scale motions during tropical cyclone intensification. Kuo (1965, 1974) also introduced parameterizations for use in tropical cyclone modeling which were subsequently employed in large-scale numerical prediction models (e.g., Krishnamurti, 1969; Krishnamurti *et al.*, 1979). Manabe *et al.* (1965) introduced an adjustment scheme to simulate subgrid-scale moist convection.

The cumulus parameterization proposed by Arakawa (1969)[2] considered the interaction of clouds and the large-scale environment through environmental subsidence induced by cumulus convection. Although rudimentary, the closure for the parameterization was the first to incorporate explicitly the concept of a quasi-equilibrium between the generation of conditional instability by the large-scale dynamical processes and its destruction by clouds.

Ooyama (1971) presented a cumulus parameterization that represented clouds as independent buoyant elements or bubbles. This parameterization first incorporated a spectrum of clouds.

More recently, Arakawa and Schubert (1974)[3] developed a cumulus parameterization which contained a spectral cloud ensemble model and a closure hypothesis based on well-defined physical assumptions. An evaluation of these assumptions using observed data is the subject of this paper. However, before proceeding to the main body of the paper, we shall review some fundamental aspects of the cumulus parameterization problem.

We define the goal of a cumulus parameterization for large-scale numerical prediction models as

[1] Current affiliation: National Hurricane Research Laboratory, NOAA, Coral Gables, FL 33146.

[2] Arakawa, A., 1969: Parameterization of cumulus convection. *Proc. WMO/IUGG Symp. Numerical Weather Prediction*, Tokyo. IV, 8, 1–6. [Available from Dept. Atmos. Sci., UCLA, 405 Hilgard Ave., Los Angeles, CA 90024].

[3] Henceforth referred to as Part I.

0022-4928/80/122677-16$08.00

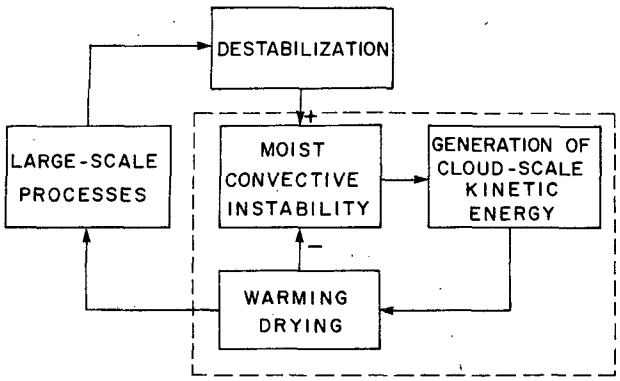


FIG. 1. A schematic diagram of the Arakawa-Schubert closure assumption. The dashed box represents the cumulus parameterization.

follows: to *predict* changes in the grid-scale variables due to subgrid-scale cumulus convection. Since, as stated earlier, the collective effects are to be parameterized, an overall measure of the intensity of subgrid-scale cumulus convection must be determined from the grid-scale variables. This determination is impossible without a closure assumption and, therefore, no parameterization is complete without one.

In order for a cumulus parameterization to be feasible, some kind of statistical balance must exist between the cumulus cloud ensemble and the grid-scale variables. If such balance does not exist it is in principle impossible to parameterize cumulus convection. Any closure assumption for cumulus parameterization, therefore, can be interpreted as an assumed balance between the cumulus cloud ensemble and the grid-scale variables. It is very important that the assumed balance be explicitly stated as a closure assumption so that it can be rationally evaluated.

The assumed balance should satisfy at least two basic principles. First, it should be universally valid since cumulus convection occurs in widely different temperature and moisture regimes in the atmosphere. Second, it should not cause the loss of predictability of any prognostic variable of the model. For example, steadiness in the grid-scale prognostic variables, such as temperature or humidity, cannot be used as the assumed balance. Although observations may show that these variables are approximately steady in some situations, this fact *must be reproduced*, rather than assumed *a priori*, by the model.

Section 2 of this paper reviews the closure assumption of the Arakawa-Schubert cumulus parameterization. Section 3 presents an evaluation of the closure assumption using observed data and Section 4 discusses the results. Section 5 gives a summary and conclusions. The discrete version of the parameterization used in this paper is described in a forthcoming paper by Lord *et al.*, referred to as Part IV. Evaluation of the parameterization using observations is continued in a forthcoming paper by Lord, referred to as Part III.

## 2. The Arakawa-Schubert cumulus parameterization

A theory of the interaction of a cumulus ensemble with the large-scale environment was fully described in Part I. Cumulus clouds are assumed to modify the large-scale environment by compensating subsidence between the clouds and by detrainment of cloud air containing suspended liquid water droplets. Since the cumulus parameterization must predict the vertical distribution of cumulus modification of the large-scale environment, the cumulus cloud ensemble is divided into subensembles according to a spectral parameter $\lambda$. The fundamental assumption in the spectral decomposition of the cloud ensemble is that $\lambda$ characterizes the statistical properties of all members of the subensemble and consequently all subensemble members modify the environment in the same manner. The specific choice for $\lambda$ is discussed in the Appendix.

Based on that assumption, the subensemble budget equations for mass, moist static energy and total water (vapor, suspended liquid water and precipitation) are derived by summation of the respective cloud budgets for all subensemble members in the large-scale area. Solution for the cloud subensemble thermodynamical properties from the vertical distribution of large-scale thermodynamical variables is achieved by normalization of the subensemble mass flux at cloud base, assumption of nonbuoyancy of cloud air at the cloud top and specification of the cloud base moist static energy and water vapor mixing ratio. Therefore, the parameterization of cumulus convection is reduced to the determination of the remaining unknown, the distribution of cloud-base mass flux $M_B(\lambda)$.

As discussed in the Introduction, a closure assumption is needed to complete any cumulus parameterization. In the Arakawa-Schubert parameterization, the closure takes the form of a balance between the generation of moist convective instability by the large-scale processes and its destruction by clouds as shown schematically in Fig. 1. Cloud-scale kinetic energy is the manifestation of a moist convective instability in the environment. The large-scale equations (74) and (75) in Part I show that environmental subsidence induced by clouds produces warming and drying in the large-scale environment, thereby decreasing the cloud buoyancy (stabilization). On the other hand, the large-scale processes, consisting of advection, boundary-layer processes and radiative cooling, can

steepen the temperature lapse rate and moisten the environment, thereby increasing the cloud buoyancy (destabilization). The closure assumption expresses the approximate balance between the stabilizing and destabilizing processes.

Let us now examine the cumulus subensemble kinetic energy budget to provide a physical interpretation of this closure assumption. For a cloud subensemble with fractional entrainment rate between $\lambda$ and $\lambda + d\lambda$, let $\mathcal{K}(\lambda)d\lambda$ be the cloud-scale kinetic energy for the subensemble, $A(\lambda)$ be the cloud-work function defined as the cloud-scale kinetic energy generation per unit $\mathcal{M}_B(\lambda)d\lambda$, and $\mathcal{D}(\lambda)$ be the cloud-scale kinetic energy dissipation per unit $\mathcal{M}_B(\lambda)d\lambda$. The kinetic energy budget for the cloud subensemble may be written as

$$\frac{d}{dt}\mathcal{K}(\lambda)d\lambda = [A(\lambda) - \mathcal{D}(\lambda)]\mathcal{M}_B(\lambda)d\lambda. \quad (1)$$

Now consider a hypothetical situation in which there is no generation of kinetic energy and, therefore, only dissipation by various processes is acting on the subensemble. Let $\tau_{\text{DIS}}$ be the decay time in this situation. Then, in terms of orders of magnitude, Eq. (1) gives

$$\mathcal{D}(\lambda)\mathcal{M}_B(\lambda) \sim \frac{\mathcal{K}(\lambda)}{\tau_{\text{DIS}}}. \quad (2)$$

Let $\tau$ be the time scale over which we apply (1). Then using (2) in (1) we have

$$\frac{\mathcal{K}(\lambda)}{\tau} \sim A(\lambda)\mathcal{M}_B(\lambda) - \frac{\mathcal{K}(\lambda)}{\tau_{\text{DIS}}}. \quad (3)$$

When $\tau \gg \tau_{\text{DIS}}$, the left-hand side (lhs) of (3), and therefore that of (1), can be neglected. Eq. (1) then gives

$$A(\lambda) \approx \mathcal{D}(\lambda) \quad \text{for} \quad \mathcal{M}_B(\lambda) > 0. \quad (4)$$

This equation is a statement of the "kinetic energy quasi-equilibrium" for each cumulus subensemble.

Eq. (4) was derived on the assumption that $\tau_{\text{DIS}} \ll \tau$. By definition, $\tau_{\text{DIS}}$ is the time scale when only dissipative processes are acting; therefore, it must be smaller than an actual cloud lifetime which includes both generation and dissipation. We thus estimate $\tau_{\text{DIS}}$ to be of order $10^2$–$10^3$ s. Since we wish to predict changes of a cumulus ensemble over the time scale of large-scale disturbances ($\tau_{\text{LS}}$) an appropriate choice for $\tau$ is $\tau = \tau_{\text{LS}}$, where $\tau_{\text{LS}}$ is typically of order $10^5$ s. Then $\tau_{\text{DIS}} \ll \tau_{\text{LS}}$ and, therefore, the kinetic energy quasi-equilibrium is a very good approximation.

The primary source of kinetic energy generation for cumulus convection is the buoyancy force even though interaction of cumulus clouds with the vertical wind shear can be important in some situations. Therefore, in Part I, the cloud-work function $A(\lambda)$ was defined as the subensemble kinetic energy generation (per unit cloud-base mass flux) due to work done by the buoyancy force, i.e.,

$$A(\lambda) = \int_{z_B}^{\hat{z}(\lambda)} \frac{g}{\bar{T}(z)}\eta(z,\lambda)[T_{vc}(z,\lambda) - \bar{T}_v(z)]dz, \quad (5)$$

where $T_{vc}(z,\lambda)$ and $\bar{T}_v(z)$ are the subensemble and environmental virtual temperatures, $\hat{z}(\lambda)$ is the subensemble cloud-top height, and $\eta(z,\lambda)$ is the subensemble normalized vertical mass flux.

It is important to note that *for a given* $\lambda$, $A(\lambda)$ *depends solely on the large-scale thermodynamical vertical structure* since the difference $T_{vc}(z,\lambda) - \bar{T}_v(z)$ is determined by the vertical structure. It was shown in Part I that $A(\lambda)$ is a generalized measure of the moist convective instability in the large-scale environment.

With this definition of $A(\lambda)$, Eq. (4) has a clear physical interpretation. If the cloud-scale kinetic energy generation by the buoyancy force is more than is needed to balance the dissipation in a statistical sense, the vertical mass flux of clouds and, correspondingly, the induced subsidence between clouds will increase. The resulting increase in the warming and drying in the environment and decrease of the subcloud layer depth will tend to reduce the moist convective instability by decreasing the buoyancy felt by the clouds. Consequently, the cumulus-scale kinetic energy generation will decrease. Thus kinetic energy generation tends to balance dissipation, $A(\lambda) \approx \mathcal{D}(\lambda)$. If $A(\lambda) < \mathcal{D}(\lambda)$ there can be no sustained convection over the large-scale area. Therefore, when $A(\lambda) < \mathcal{D}(\lambda)$, $\mathcal{M}_B(\lambda) = 0$ and (4) does not apply. This situation has been discussed in detail in Part I.

In general, dissipation in clouds should depend primarily on momentum entrainment through cloud boundaries and downward drag due to precipitation falling within the cumulus updrafts. Regardless of the details of the dissipation mechanisms, however, the total dissipation should be roughly proportional to the cloud mass flux. Then $\mathcal{D}(\lambda)$, which is the dissipation *per unit cloud-base mass flux,* will not depend substantially on the large-scale situation once the cloud type (i.e., $\lambda$) is specified. In other words, to a first order of approximation, $\mathcal{D}(\lambda)$ can be regarded as an intrinsic cloud subensemble property and hence is a quasi-constant for each cloud type.

We have shown that for a given $\lambda$, $A(\lambda)$ depends solely on the large-scale thermodynamical vertical structure. On the other hand, $\mathcal{D}(\lambda)$ is an intrinsic cloud subensemble property. The kinetic energy quasi-equilibrium (4) thus hypothesizes a remarkable relationship between the large-scale thermodynamical vertical structure and the cloud-scale

dissipation. This relationship clearly depends on the large-scale vertical structure of both temperature *and* moisture. Therefore, the kinetic energy quasi-equilibrium regulates a coupled temperature and moisture structure in the large-scale environment. It does *not* imply that temperature and moisture are constrained individually.

To derive a practicable closure assumption, we take the derivative of (4) with respect to a time long enough for the kinetic energy quasi-equilibrium to hold. Then

$$\frac{d}{dt}A(\lambda) \approx \frac{d}{dt}\mathcal{D}(\lambda). \tag{6}$$

Based on the above argument, we may set

$$\frac{d}{dt}\mathcal{D}(\lambda) \approx 0, \tag{7}$$

even when a cumulus ensemble is not in an exactly steady state. Then from (6),

$$\frac{d}{dt}A(\lambda) \approx 0. \tag{8}$$

This constraint on $A(\lambda)$ can be used as a closure assumption as described below.

The time derivative of $A(\lambda)$ in (8) can be separated into two parts, one representing the effects of cumulus feedback on the large-scale fields and the other representing the effects of the large-scale processes. Then (8) becomes

$$\left[\frac{d}{dt}A(\lambda)\right]_{CU} + \left[\frac{d}{dt}A(\lambda)\right]_{LS} = \frac{d}{dt}A(\lambda), \tag{9a}$$

$$\approx 0, \tag{9b}$$

where the subscript $CU$ refers to cumulus effects. Eq. (9b) is a statement of cumulus ensemble "cloud-work function quasi-equilibrium".

In Part I, the following integral equation for $\mathcal{M}_B(\lambda)$ was derived from (9b) in a relatively straightforward manner:

$$\int_0^{\lambda_{max}} K(\lambda,\lambda')\mathcal{M}_B(\lambda')d\lambda' + F(\lambda) = 0, \tag{10}$$

where $K(\lambda,\lambda')$ is the mass flux kernel and the large-scale forcing $F(\lambda)$ is defined as $[dA(\lambda)/dt]_{LS}$. Therefore, the assumption of the cloud-work function quasi-equilibrium (9b) has closed this cumulus parameterization. Observational evidence for the cloud-work function quasi-equilibrium is presented in the next section and in Part III.

Fig. 2 summarizes the closure assumption of the Arakawa-Schubert parameterization. The sub-ensemble kinetic energy equation (1) relates the time change of the subensemble kinetic energy to the generation of kinetic energy by buoyancy forces and the dissipation by various processes. The kinetic energy quasi-equilibrium (4) asserts the balance of kinetic energy generation and dissipation when generation is sufficient to balance dissipation and the nonexistence of sustained convection other-

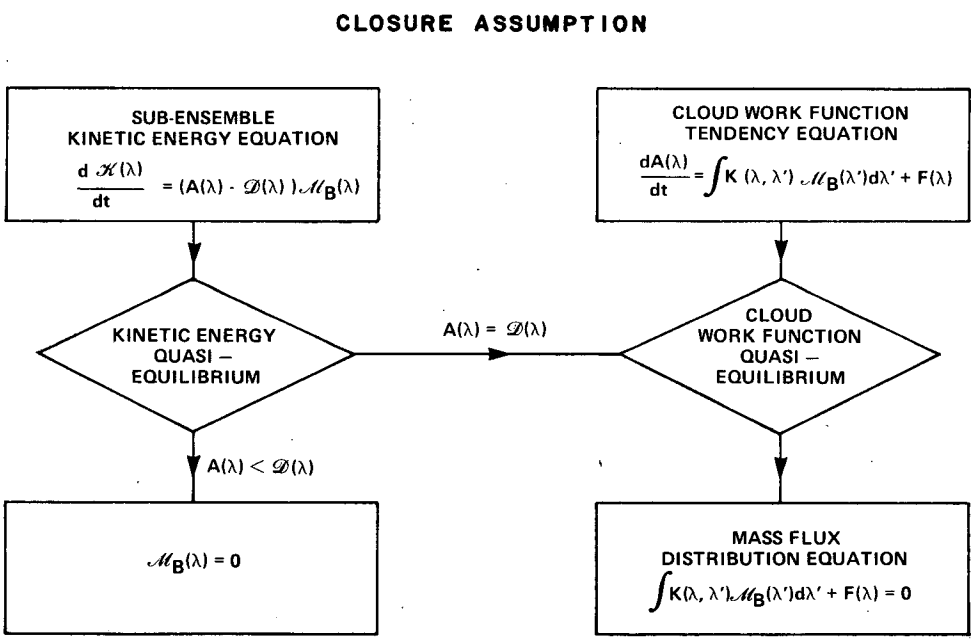


FIG. 2. A summary of the derivation of the mass flux distribution equation (10) using the kinetic energy quasi-equilibrium and the cloud-work function quasi-equilibrium.

wise. The cloud-work function tendency equation (9a) describes the changes in $A(\lambda)$ due to large-scale and cumulus processes. The cloud-work function quasi-equilibrium (9b), which holds when the dissipation in clouds per unit cloud-base mass flux is primarily a function of cloud type, results in the equation for the mass flux distribution function.

We now summarize this section with Fig. 3 which is a schematic diagram showing the logical structure of this cumulus parameterization. The parameterization (diamond boxes) relates the large-scale variables and processes (upper rectangular boxes) to those of the cumulus-scale (lower rectangular boxes). The large-scale model contains the advective processes and the parameterized radiation and boundary-layer processes. The subensemble thermodynamical budgets determine the subensemble thermodynamical properties from the large-scale thermodynamical structure. The closure assumption determines the subensemble mass flux distribution function from the large-scale processes and the mutual interaction of the subensembles. The mass flux distribution function and the subensemble thermodynamical properties together determine the cumulus feedback on the large-scale thermodynamical structure through the environmental thermodynamical budgets.

## 3. The cloud-work function calculated from observations

In the previous section, it was argued that the dissipation per unit cloud-base mass flux $\mathcal{D}(\lambda)$ is (to a first approximation) an intrinsic property of each cumulus subensemble. Therefore, it should be a quasi-constant for each cloud type and should not depend on individual synoptic situations. In light of the kinetic energy quasi-equilibrium, $A(\lambda) \approx \mathcal{D}(\lambda)$, values of the cloud work function $A(\lambda)$ should also be quasi-constant *whenever* that type of cloud exists. Since $A(\lambda) < 0$ implies that those cumulus clouds are not generated, the constraint (4) does not hold for negative values of $A(\lambda)$.

In this study, values of the cloud-work function are calculated from observations over a wide variety of synoptic conditions in the tropics and subtropics. Since vertical profiles of temperature and moisture are the only data needed for this calculation, radiosonde measurements are sufficient for this study. However, some averaging of the data in space and/or time is performed to give values of temperature and moisture that are more representative of a large-scale area. The next section briefly describes each data set used in this study and the type of averaging performed on each data set.

### *a. The data*

We have used data from the seven different locations and synoptic conditions in the tropics and subtropics shown in Fig. 4. The data sets are described below.

#### 1) THE MARSHALL ISLANDS DATA SET

The Marshall Islands data set has been described by Yanai *et al.* (1973) and Chu (1976).[4] The data were taken from a set of 6 hourly (0300, 0900, 1500 and

[4] Chu, J.-H., 1976: Vorticity in maritime cumulus clouds and its effects on the large-scale budget of vorticity in the tropics. Ph.D. thesis, UCLA, 123 pp.

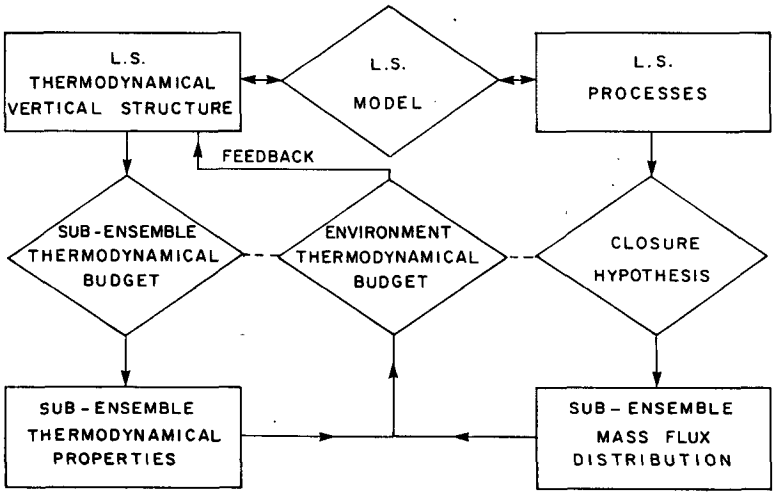


FIG. 3. A schematic diagram showing the logical structure of the complete Arakawa-Schubert cumulus parameterization.

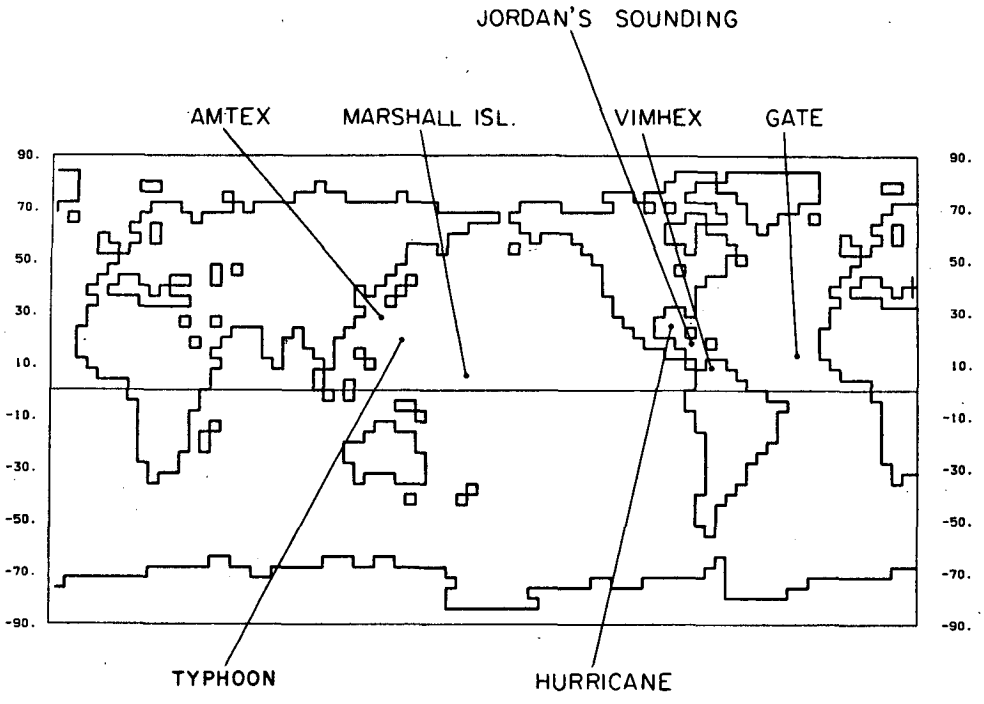


FIG. 4. Locations of the data sets used in the calculations of cloud-work functions from observations.

2100 GMT) upper air and surface observations from Operation Redwing which took place in the Marshall Islands area from 15 April to 22 July 1956. Temperatures ($T$), relative humidities ($r$) and heights ($z$) were given at 50 mb pressure intervals from 1000 to 100 mb at the eight stations shown in Fig. 5. Water vapor mixing ratios ($q_v$) were calculated at each station from $r$ using the Goff-Gratch formula (*Smithsonian Meteorological Tables*, 6th rev. ed.). The eight stations were used to subdivide the entire area into six triangular areas. At each observation time and pressure level, $q_v$ and $z$ were averaged over the three stations at the vertices of each triangle to give a representative value for each triangle. These values were then time averaged with a 1-2-1 weighting over 12 h to produce a total of 2322 observations at 6 h intervals. Following Yanai *et al.* (1976) these observations were further separated into "disturbed" cases and "undisturbed cases" according to the sign of $\bar{\omega}$ in the layer between 300 and 400 mb.

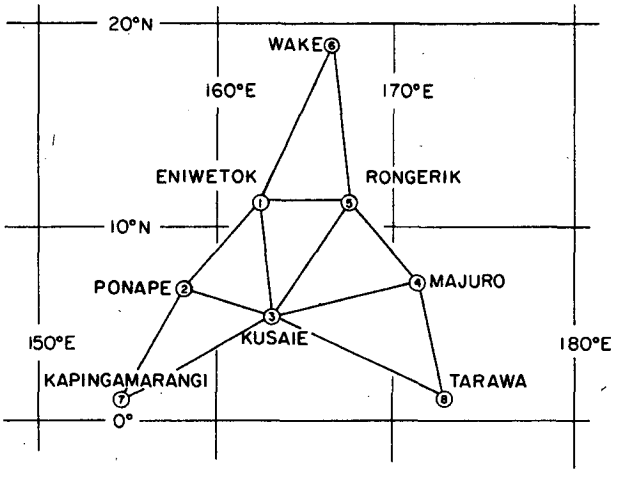


FIG. 5. Locations of the eight stations of the Marshall Islands data set. Six large-scale areas were defined by averaging data from stations at the vertices at each triangle.

### 2) VIMHEX DATA SET

The Venezuelan International Meteorological and Hydrological Experiment (VIMHEX-1972) has been described by Betts and Miller (1975).[5] The rawinsonde data used in this study were taken from a single land station in north-central Venezuela from 22 May–6 September 1972. A total of 328 observations from this data set were used. Values of temperature and mixing ratio at the surface and at 25 mb pressure intervals from 975 to 150 mb (or the sounding termination level if lower) were reported for each observation time. These data were averaged vertically by a 1-2-1 weighting over 50 mb intervals to reduce observational noise.

[5] Betts, A. K., and R. D. Miller, 1975: VIMHEX-1972 rawinsonde data. Atmos. Sci. Res. Report, Colorado State University.

The VIMHEX was designed to study the local structure of the atmosphere in the near vicinity of mesoscale convective systems propagating over this area. Consequently, most soundings were taken in close proximity to precipitating convection and this sampling procedure could lead to large variations in the individual soundings. The irregular sampling time used in the VIMHEX made it inappropriate to time-smooth the data and, since only a single station was reported, space-smoothing was impossible.

### 3) GATE DATA SET

The GARP Atlantic Tropical Experiment (GATE) was held in the tropical eastern Atlantic Ocean during the summer of 1974. The data used in this study are those analyzed by method 2 of Thompson *et al.* (1979). Temperature and specific humidity were given for the center of the B-scale array at 25 mb intervals from 1000 to 100 mb.[6] There were 152 observation times at 3 h intervals from 0000 GMT 31 August to 2100 GMT 18 September. The heights of each pressure surface were calculated hydrostatically from the temperature and mixing ratio at each observation time.

[6] Moisture data above 300 mb were not analyzed by Thompson *et al.* (1979). We have assumed a 50% relative humidity above 300 mb.

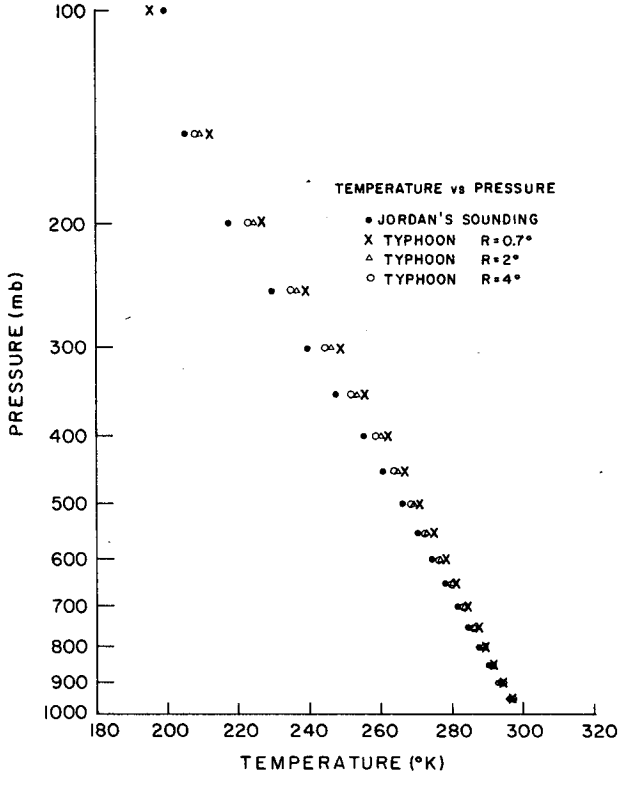


FIG. 6. Temperature (K) versus height (mb) for Jordan's (1958) mean West Indies sounding and the composited typhoon data.

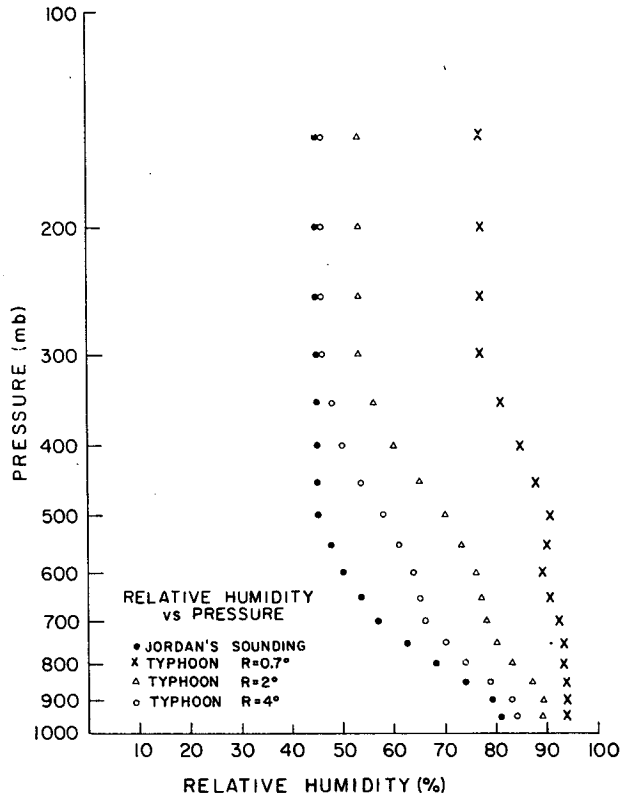


FIG. 7. Relative humidity (%) versus height (mb) for Jordan's (1958) mean West Indies sounding and the composited typhoon data.

### 4) AMTEX DATA SET

The AMTEX upper air data were collected from four stations in the East China Sea during two separate two-week periods of 14–28 February 1974 and 14–28 February 1975, and were processed as described by Nitta (1976). The processed data set consisted of temperature and mixing ratio averaged over the four stations at the surface and at 25 mb intervals from 1000 to 100 mb. There were 117 observation times at 6 h intervals over both AMTEX periods. These data were then smoothed vertically as in the VIMHEX data. Time-averaging for this data set was not performed due to the relatively small number of observations.

### 5) MEAN WEST INDIES TROPICAL SOUNDING

The West Indies mean sounding for the hurricane season (July–October) was taken from Jordan (1958). He calculated the mean data from nighttime

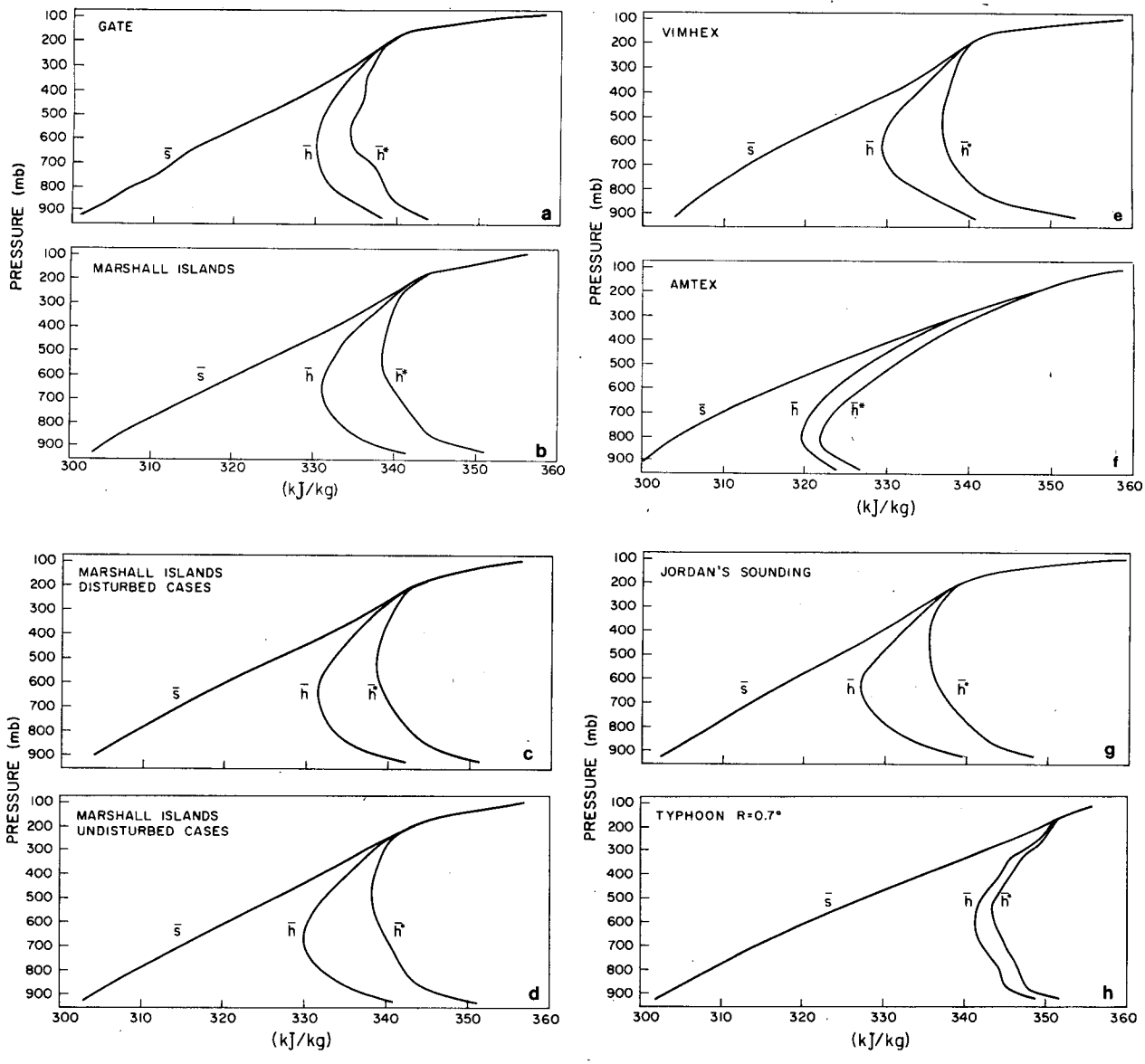


FIG. 8. Average dry static energy ($\bar{s}$), moist static energy ($\bar{h}$) and saturation moist static energy ($\bar{h}^*$) versus pressure (mb) for all data sets used to calculate the cloud-work function: (a) GATE; (b) Marshall Islands; (c) Marshall Islands "disturbed" cases; (d) Marshall Islands "undisturbed" cases; (e) VIMHEX; (f) AMTEX; (g) Jordan's (1958) mean West Indies sounding; (h) composited typhoon, $R = 0.7°$ latitude; (i) typhoon $R = 2°$; (j) typhoon, $R = 4°$; (k) composited hurricane, $R = 2°$; (l) hurricane, $R = 4°$; (m) hurricane, $R = 6°$.

soundings at Miami, San Juan and Swan Island in the Caribbean Sea over a 10-year period (1946–55). Values of temperature at the surface and every 50 mb from 950 to 100 mb were given with corresponding values of $r$ from the surface to 450 mb. Above 450 mb, $r$ was assumed to be the same as the value at 450 mb (42%). These data were then linearly interpolated to give values at the 975, 925, . . . , 175, 125 mb levels and $q_v$ was calculated from the Goff-Gratch formula as described above.

### 6) COMPOSITED NORTHWEST PACIFIC TYPHOON

A set of composited typhoon data from the Northwest Pacific has been described by Frank (1977). He used approximately 18 000 soundings from 30 stations over a 10-year period (1961–70) in the compositing analysis. The compositing was performed for a 15° latitude radius, cylindrical grid located at the storm center and extending from sea level to 50 mb. The composited soundings of $T$ and $r$

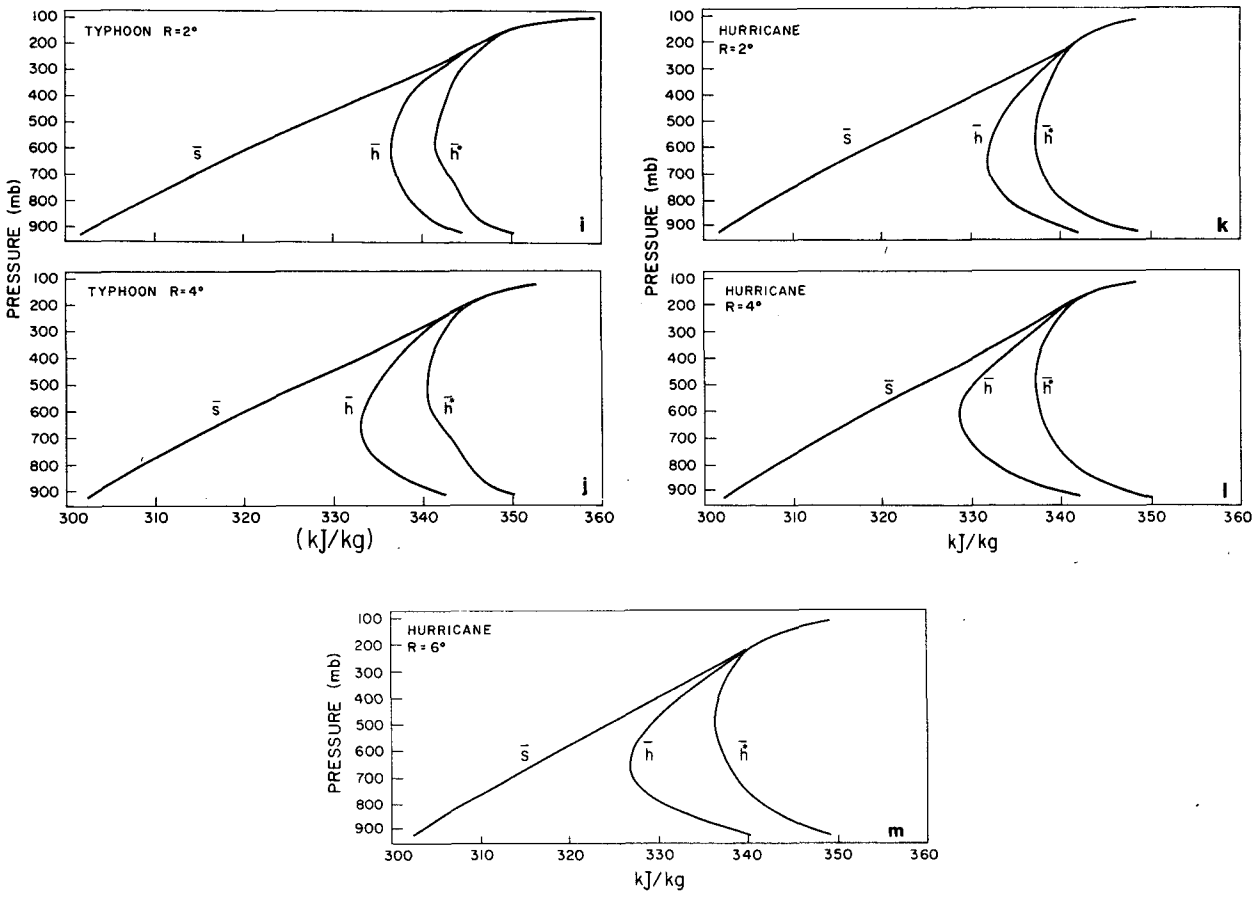


FIG. 8. *(Continued)*

centered at radii $R = 0.7$, 2 and 4° latitude were used in this observational study. Temperature data were given at the surface and at 50 mb intervals between 100 and 300 mb and between 800 and 950 mb; temperatures between 300 and 800 mb were given at 100 mb intervals. Relative humidity was given at the corresponding pressure levels up to 300 mb and above 300 mb, it was assumed to be the same as the 300 mb value. Linear interpolations were used to fill in the data to 25 mb intervals and $q_v$ was calculated as described previously.

### 7) COMPOSITED WEST INDIES HURRICANE DATA

The West Indies composited hurricane data were derived from observations at 52 coastal and island stations in the Gulf of Mexico and the Caribbean Sea bounded on the north by the Bahamas and on the east by the Lesser Antilles (Nunez and Gray, 1977).[7] All disturbances with winds > 65 kt over a 14-year period from 1961–74 were included in the composite analysis. The compositing procedure by Nunez and Gray was similar to that for the typhoon data described above. Soundings centered at $R = 2$, 4 and 6° were used in this study. Temperature and relative humidity were given every 50 mb between 100 and 400 mb and between 800 and 950 mb, and every 100 mb between 400 and 800 mb. Again, linear interpolations were used to fill in the data to 25 mb intervals and $q_v$ was calculated as described previously.

The temperature and relative humidity versus pressure for Jordan's mean sounding and the composited typhoon soundings at $R = 0.7$, 2 and 4° are shown in Figs. 6 and 7. Substantial differences in the static stability and humidity between the soundings are evident. The static stability increases proceeding from Jordan's sounding to regions closer to the center of the typhoon. The relative humidity changes by as much as 40% in the middle troposphere proceeding from the relatively dry mean state to the very humid air near the center of the typhoon.

The time-averaged soundings for all data sets used

[7] Nunez, E., and W. M. Gray, 1977: A comparison between West-Indies hurricanes and Pacific typhoons. *Preprints 11th Tech. Conf. Hurricanes and Tropical Meteorology*, Miami Beach, Amer. Meteor. Soc.

in this study are shown as profiles of $\bar{s}$, $\bar{h}$ and $\bar{h}^*$ from 100 to 950 mb in Figs. 8a–8m. Comparison of these profiles indicates some striking differences. The Marshall Islands area shows a relatively dry middle troposphere compared to the GATE area and is somewhat more dry adiabatically stable than the VIMHEX area in the time average. There is very little difference between the Marshall Islands "disturbed" and "undisturbed" profiles. The time-averaged AMTEX sounding shows a very shallow layer of conditional instability and is completely different from each of the other data sets used in this study. We have already noted the very large differences between Jordan's sounding and the composite typhoon soundings at radii $R = 0.7$, 2 and 4°. The hurricane soundings show a similar trend to the typhoon soundings.

### b. The procedure

When the Arakawa-Schubert parameterization is vertically discretized, it is convenient to classify cloud types into subensembles by the cloud top pressure level $\hat{p}$, rather than by the fractional entrainment rate, $\mu$. Therefore $\lambda = \hat{p}$ as discussed in the Appendix. The discrete model used in this study has 17 possible cloud types with cloud-top levels at 100, 150, 200, . . . , 800, 850, 912.5 mb. For simplicity the cloud-base moist static energy and water vapor mixing ratio are given by their respective values at 950 mb and the subcloud layer top is chosen to be at 950 mb for all data.

For each data set the cloud subensemble properties, including $\mu$ and $A(\lambda)$ are determined following the procedure described in Part IV. For all cloud types the precipitation parameter is $c_0 = 2.0 \times 10^{-3}$ m$^{-1}$. A parameterized ice phase is used as described by Lord (1978).[8] For the Marshall Islands, VIMHEX and GATE data sets, the means and standard deviations of $A(\lambda)$ are calculated for each cloud type and each data set. All values of $A(\lambda)$ greater than three standard deviations from the mean are discarded and the means and standard deviations are recalculated. Negative cloud-work

[8] Lord, S. J., 1978: Development and observational verification of a cumulus cloud parameterization. Ph.D. dissertation, UCLA, 359 pp.

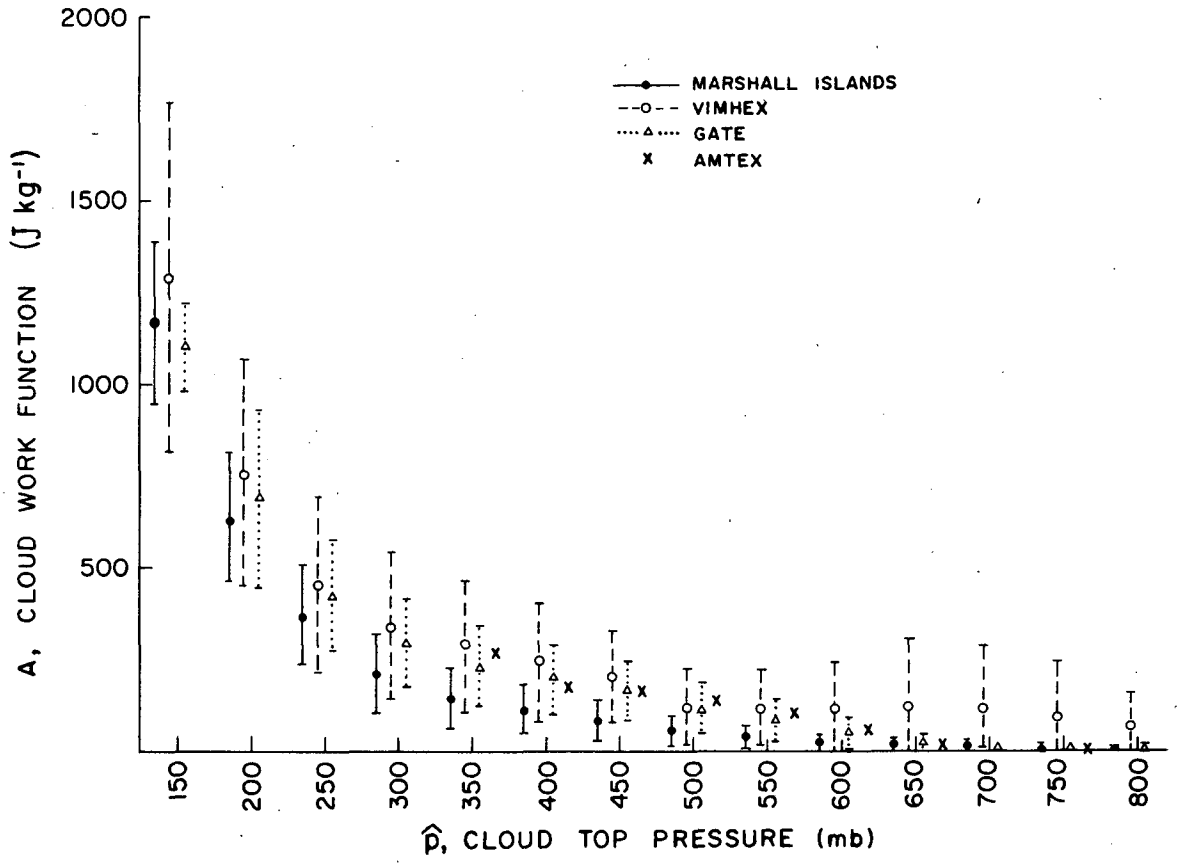


FIG. 9. Mean values and standard deviations of the cloud-work function versus cloud-top pressure $\hat{p}$ calculated from the Marshall Islands, VIMHEX, GATE and AMTEX data sets. Error bars represent one standard deviation from the mean.

functions are not included in the analysis. Details concerning the sensitivity of the parameterization to the cloud base conditions and the formulation of the cloud ensemble model are discussed in Part III.

### c. *The results*

Fig. 9 shows the mean cloud-work function values grouped according to cloud-top pressure for the Marshall Islands, VIMHEX, GATE and AMTEX data sets. "Error" bars represent one standard deviation from the mean. Standard deviations were not calculated for AMTEX because of the small number of positive cloud-work functions. Fig. 10 is the same type of graph for the Marshall Islands "disturbed" and "undisturbed" cases, Jordan's sounding and the various typhoon soundings. Fig. 11 shows results from the composite hurricane soundings; the typhoon $R = 2°$ results and the GATE results have been included for comparison.

In Fig. 9 the mean cloud-work functions from the Marshall Islands lie within the error bars for the GATE for all cloud types. The mean values for AMTEX, although derived from only a few cases, are very close to the GATE mean values. The mean cloud-work functions for VIMHEX are consistently higher than the means for the other data sets and the standard deviations are much larger. Even so, the error bars for VIMHEX encompass the mean values for each of the other areas.

Fig. 10 shows that there is virtually no difference between the "disturbed" and "undisturbed" cases for the Marshall Islands data except for the deepest 150 mb clouds that have somewhat different standard deviations. The cloud-work functions for Jordan's sounding are close to the Marshall Islands averages for clouds with tops below 250 mb. The typhoon cloud-work functions increase consistently toward the cyclone center for clouds with tops below 250 mb but are nevertheless confined within the narrow ranges defined by the other data. The values for $R = 2°$ and $R = 4°$ lie very close to the mean values of the other data sets and within the error bars of *all* other data sets. The $R = 0.7°$ values are consistently larger for clouds with tops between 300 and 600 mb but still lie within the error bars for GATE.

The hurricane results shown in Fig. 11 give cloud-work functions for $R = 2, 4$ and $6°$. As in the typhoon cases, regions closer to the hurricane center show

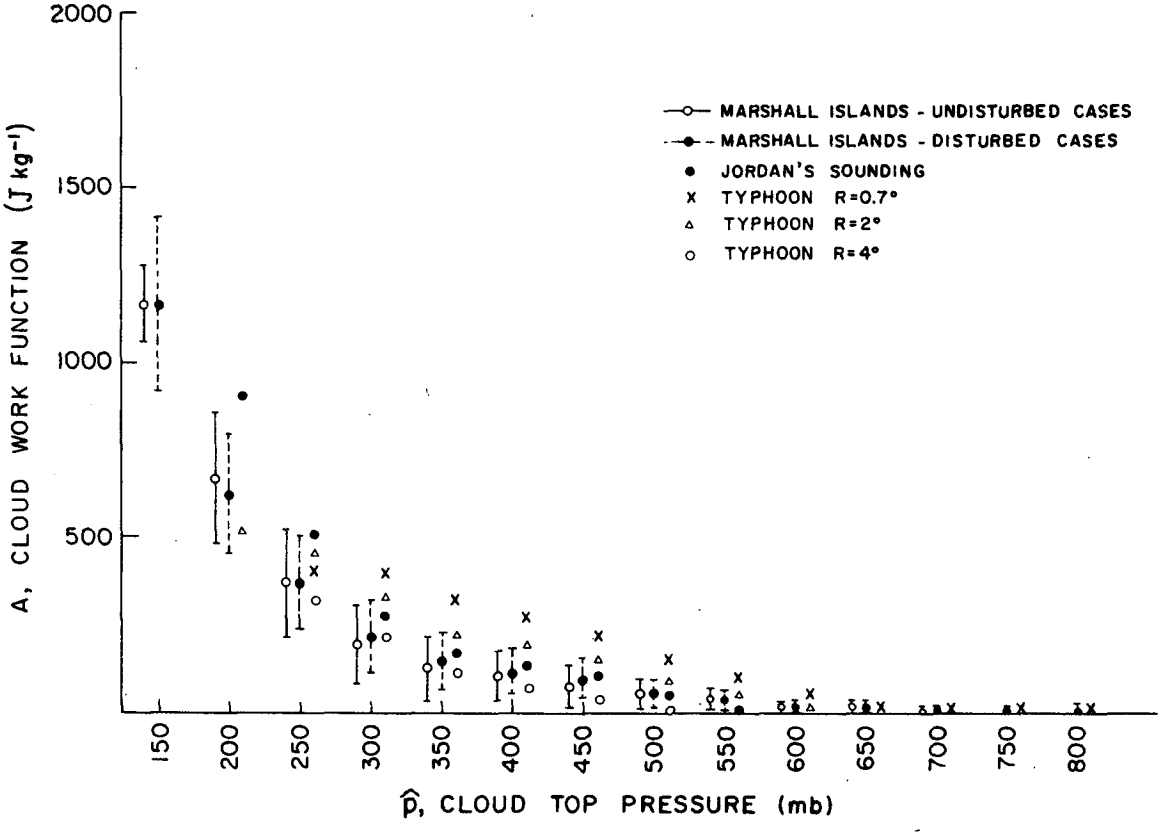


FIG. 10. As in Fig. 9 except for the Marshall Islands undisturbed and disturbed cases, Jordan's sounding, and the composited typhoon data at $R = 0.7$, 2 and 4°.

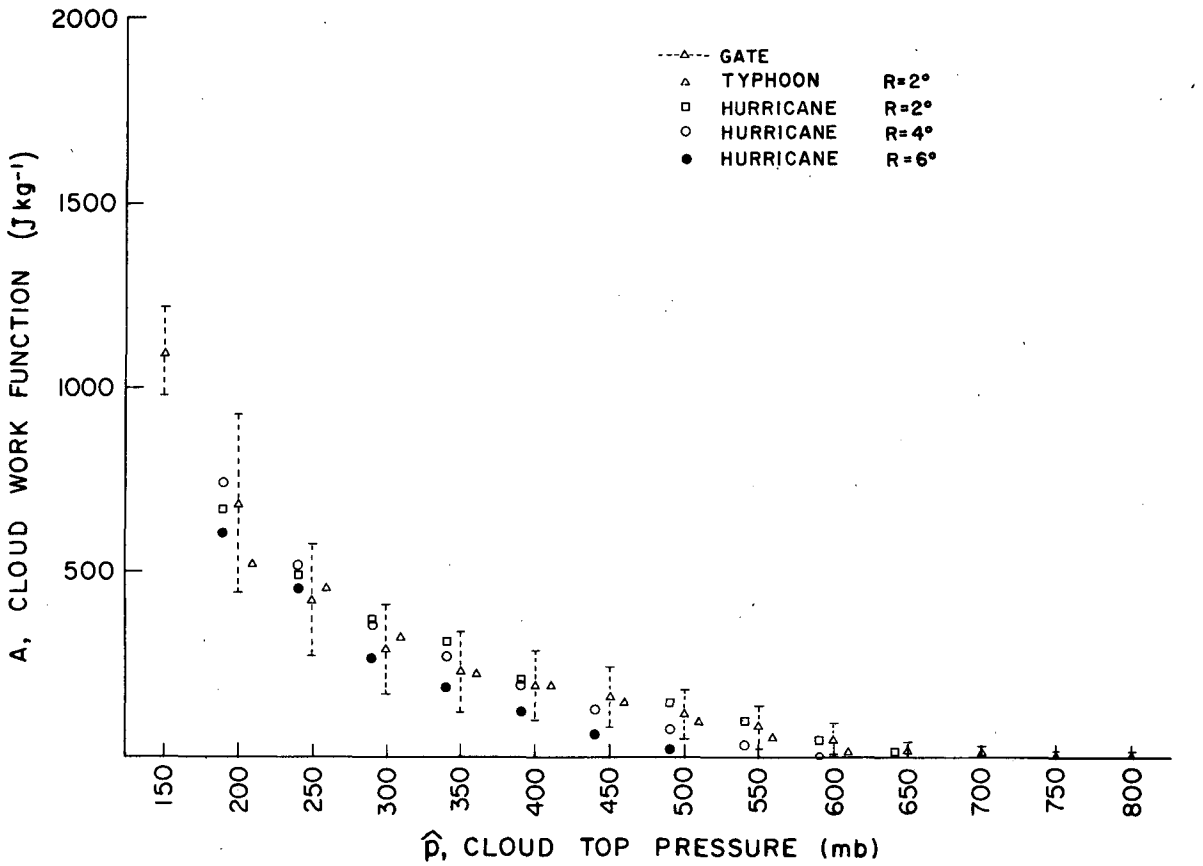


FIG. 11. As in Fig. 9 except for the composited hurricane data at $R$ = 2, 4 and 6°. The GATE mean values and the $R$ = 2° results are included for comparison.

generally higher values of the cloud-work function. In general, there is very good agreement between the two composite data sets for each radius. The hurricane results are very close to the GATE mean values for most cloud types.

## 4. Discussion

In view of the large differences in static stabilities and relative humidity distributions between these areas (see Figs. 6 and 7) the similarity in cloud-work function statistics is remarkable. The time and space-averaged cloud-work functions differ very little between a region a few hundred kilometers from the center of a tropical cyclone, an undisturbed synoptic situation in the Marshall Islands, and the AMTEX area. Indeed, the cloud-work functions shown here are quasi-constant for each cloud type.

It is also very clear from this study that the small differences in cloud-work function values are not necessarily the consequence of small differences in both the temperature and moisture fields. For example, there are large differences in temperature and moisture between the $R$ = 2° typhoon sounding and the Marshall Islands average sounding but the respective values of the cloud-work function are quite comparable.

We must also discount the notion that the cloud-work function is insensitive to changes in the large-scale variables. For example, if we maintain the observed temperature profile for the $R$ = 2° typhoon sounding but artificially modify the observed relative humidity by 5% increments, the cloud-work functions change significantly for all cloud types as shown in Fig. 12. In fact, a change of 5% in relative humidity, which is smaller than the differences in relative humidity between the typhoon soundings, is sufficient to place the cloud-work functions outside the typical ranges for each cloud type shown in Figs. 9–11. Other results, not shown here for the sake of brevity, have shown that very large variations of $A(\lambda)$ occur for the AMTEX data when the observed temperature profile is fixed but the relative humidity profile is changed by ±1 standard deviation calculated from the time series of the observed values. Similar results have been obtained by fixing the observed moisture profile and artificially changing the temperature lapse rate.

Among the data sets used in this study, the VIMHEX data provides the most demanding test of

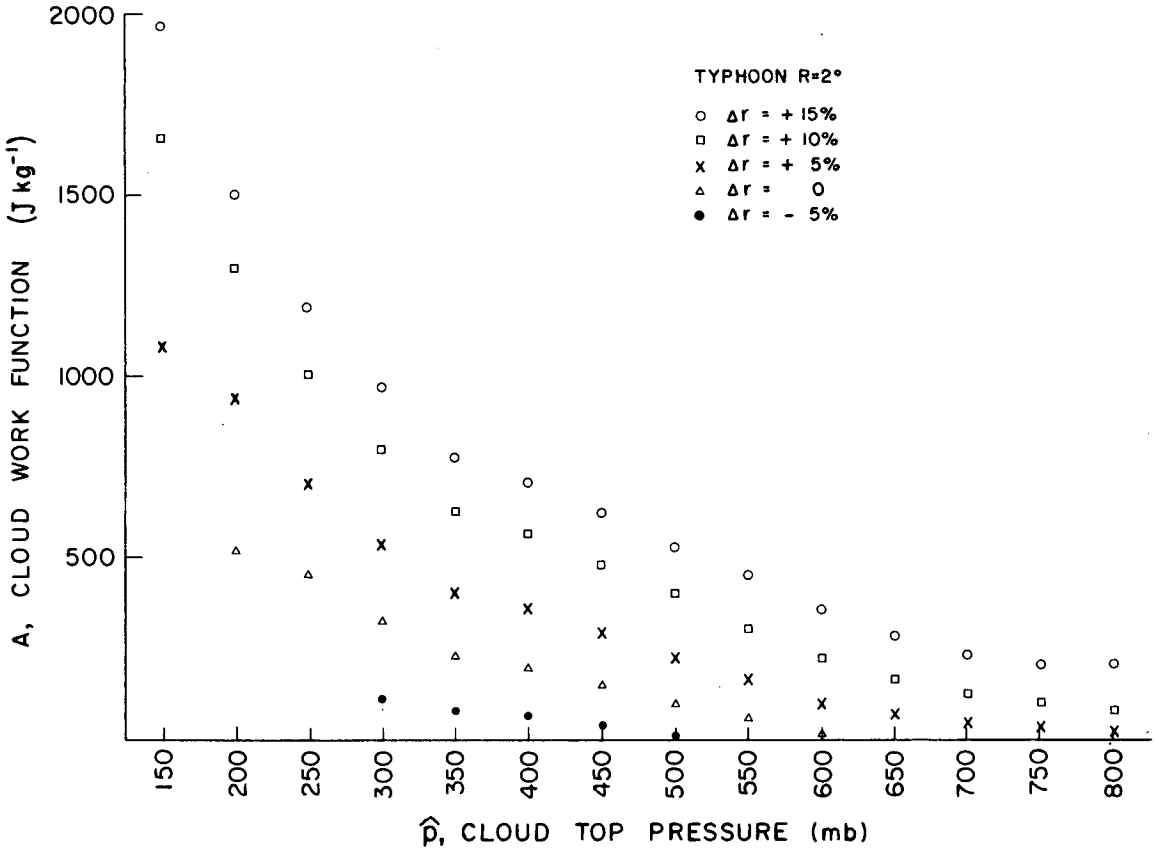


FIG. 12. As in Fig. 9 except for the typhoon $R = 2°$ case with the relative humidity artificially modified by increments of 5% while maintaining the observed temperature profile. The unmodified $R = 2°$ results are included for comparison.

the cloud-work function quasi-equilibrium. Since individual soundings are used these observations cannot be assumed representative of large-scale average values. The larger time variation of cloud-work functions therefore results. Nevertheless, the mean cloud-work function values for clouds with tops above 550 mb remain very close to the GATE and AMTEX values. The larger mean values for shallower cloud types are the result of comparatively large cloud-work functions calculated for soundings which showed an almost saturated atmosphere at these lower levels. Time or space averaging of data from the VIMHEX area would certainly produce smaller mean values and standard deviations.

The small differences between the cloud-work functions for each subensemble may be interpreted as evidence for the strong coupling between the temperature and moisture fields when cumulus clouds exist. In Part I, it was shown that $A(\lambda)$ can be written as[9]

$$A(\lambda) = \int_{z_B}^{\hat{z}(\lambda)} \rho(z)\beta(z)\Big[h_M - \bar{h}^*(z_{B+}) + \int_{z_{B+}}^{z} \eta(z',\lambda)\Big\{\lambda[\bar{h}(z') - \bar{h}^*(z')] - \frac{\partial \bar{h}^*(z')}{\partial z'}\Big\}dz'\Big]dz, \quad (11)$$

where

$$\rho(z)\beta(z) = \frac{g}{c_p\bar{T}(z)[1 + \gamma(z)]},$$

and $\gamma = (L/c_p)(\partial \bar{q}_v^*/\partial T)_p$. The $-\partial \bar{h}^*/\partial z'$ term can be written as $c_p[1 + \gamma(z')](\Gamma - \Gamma_M)$, where $\Gamma$ is the lapse rate in the environment and $\Gamma_M$ is the moist adiabatic lapse rate. When $h_M \doteq \bar{h}^*(z_{B+})$, where $z_{B+}$ indicates the level just above cloud base, $A(\lambda)$ is approximately given by a weighted double integral over the cloud height of a quantity $B(z')$ composed of two opposing terms:

$$B(z') = c_p[1 + \gamma(z')](\Gamma - \Gamma_M) + \lambda L[\bar{q}_v(z') - \bar{q}_v^*(z')]. \quad (12)$$

[9] Virtual temperature effects are ignored.

The first term is positive when the lapse rate exceeds the moist adiabatic lapse rate. Therefore, it measures the degree of conditional instability. The second term is proportional to the saturation deficit of the water vapor mixing ratio and is generally negative. Therefore, the fact that the cloud-work function is a quasi-constant for each cloud type implies the following: when cumulus convection exists, a relatively dry atmosphere has a larger lapse rate than a more moist atmosphere. The vertical thermodynamical profiles shown in Figs. 6 and 7 support this interpretation. Jordan's sounding has the largest lapse rate and also has the lowest relative humidity at each level; the relative humidity is highest and the air is the most stable near the center of the tropical cyclone. We also note that differences in relative humidity between each of these soundings are about 10%. These differences are sufficient to produce very large changes in the cloud-work function for a given temperature profile as seen from Fig. 12.

These results may also be interpreted in light of the kinetic energy quasi-equilibrium. From (4) the observed values of the cloud-work function are approximately equal to $\mathscr{D}(\lambda)$; the results therefore support our hypothesis that $\mathscr{D}(\lambda)$ has characteristic values for each cloud type under widely varying synoptic conditions. These results are also in agreement with evidence presented in Part I supporting the cloud-work function quasi-equilibrium as explained below.

The order of magnitude of $dA(\lambda)/dt$ in (9) may be estimated by considering the typical variations of $A(\lambda)$, $\delta A$, as shown in Figs. 9–11. As an extreme example, let us assume that the change of $A(\lambda)$ from Jordan's sounding to $R = 2°$ in the hurricane takes place over a period $\tau = 1$ day. For 350 mb clouds, we estimate $dA(\lambda)/dt \sim \delta A/\tau = 0.15$ kJ kg$^{-1}$ day$^{-1}$. Although there are presently no estimates of the large-scale forcing for hurricanes, Part I has shown observed forcings of approximately 4 kJ kg$^{-1}$ day$^{-1}$ from the Marshall Islands and Part III will show similar magnitudes during disturbed conditions over the GATE area. These are clearly conservative estimates of the forcing in hurricanes but they still illustrate that, in orders of magnitude,

$$\left|\frac{dA(\lambda)}{dt}\right| \ll F(\lambda). \tag{13}$$

Similar arguments can be made for other data sets if the standard deviation is taken as a measure of the variation of $A(\lambda)$ over a large-scale disturbance and 1 day is again used as the relevant time scale for the change of $A(\lambda)$. The small variability of the cloud-work function is used when this cumulus parameterization is applied to large-scale numerical prediction models (see the discussion in Part IV). Further discussion of the cloud work function variability in time for the GATE data set is given in Part III.

## 5. Summary and conclusions

The goal of a cumulus parameterization is to predict the changes in the grid-scale variables due to subgrid-scale cumulus clouds. A closure assumption, which can be interpreted as a balance between the cumulus cloud ensemble and the grid-scale variables, is necessary to complete the parameterization. The closure assumption should be a universally valid principle which does not impair the predictability of the large-scale variables.

The Arakawa-Schubert cumulus parameterization is reviewed in light of the above fundamental considerations. The closure assumption is derived from a kinetic energy quasi-equilibrium for the cumulus ensemble which expresses a near balance between the generation of kinetic energy by large-scale processes and dissipation by various cumulus processes. It is then concluded that the dissipation should depend primarily on cloud type and, consequently, cloud-work functions calculated under different synoptic conditions should be quasi-constant for each cloud type.

The results of Section 3 support this conclusion. Cloud-work functions calculated from a variety of data sets in the tropics and subtropics fall into a well-defined narrow range for each cloud type although the various thermodynamical vertical structures are quite different. Section 4 points out that this quasi-constancy of the cloud-work function implies a coupling between the vertical temperature and moisture structures in the large-scale environment due to cumulus convection.

*Acknowledgments.* This paper is based on a Ph.D. dissertation submitted by one of us (SJL) to the University of California, Los Angeles. We would like to thank those who provided the observed data used in this research: Professor Alan Betts and Dr. William Frank while at Colorado State University; Dr. Tsuyoshi Nitta, Tokyo University; and Professors Richard Reed, University of Washington, and Michio Yanai, UCLA. Thanks are due to Kurt Roberts for data processing assistance, Julia Lueken for typing the manuscript and Beverly Gladstone for drafting the figures. We thank Duane Stevens and the anonymous reviewers for their helpful comments especially regarding Section 2.

This research was supported by the Climate Dynamics Program of the National Science Foundation under Grant ATM 78-01922, by the Office of Naval Research through the Naval Environmental Prediction Research Facility under Grant N00014-78-C-0103 and by the National Aeronautics and

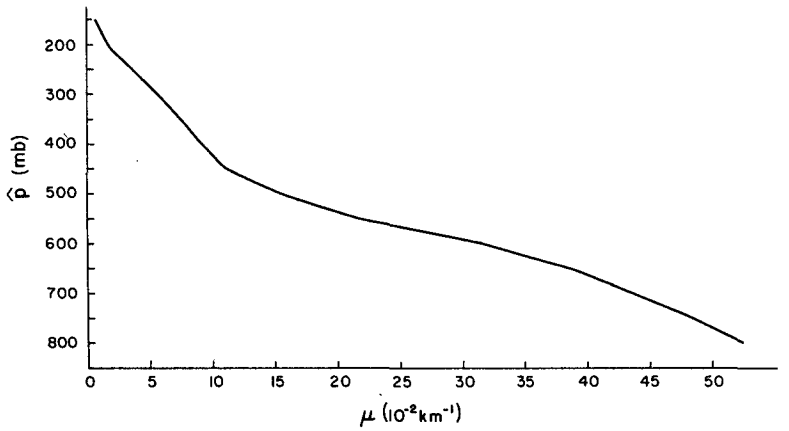


FIG. A1. Cloud-top pressure level (mb) versus average fractional entrainment rate ($10^{-2}$ km$^{-1}$) for the GATE data.

Space Administration through the Goddard Space Flight Center, Institute for Space Studies, under Grant NGR 05-007-328. Computing assistance was obtained from the UCLA Computing and Information Systems—Campus Computing Services.

## APPENDIX

### Choice of the Spectral Parameter

The fundamental assumption for the spectral decomposition of the cloud ensemble into subensembles is that a single spectral parameter $\lambda$ characterizes the statistical properties of all members of the subensemble for a given large-scale environment. Since the cloud thermodynamical properties are highly influenced by dilution of cloud air due to entrainment, Part I chose $\lambda$ to be the fractional rate of entrainment $\mu$ which was assumed constant in height. Therefore, in that paper, $\lambda \equiv \mu$. However, the choice of spectral parameter is not unique and considerable convenience in the calculations results when the cloud-top pressure $\hat{p}$ is chosen as the spectral parameter, i.e., $\lambda = \hat{p}$. In the remainder of this Appendix, we compare results of the GATE data analyzed using $\lambda = \mu$ as the spectral parameter with the results presented in Section 3.

Fig. A1 shows the cloud-top pressure $\hat{p}$ versus the average $\mu$ for the GATE data. Fig. A2 shows the mean cloud-work function values for GATE when $\lambda = \mu$ is used as the spectral parameter. Otherwise, the notation is the same as in Fig. 9. Inspection of Figs. 9 and A2 shows that the mean cloud-work function values are virtually the same for the

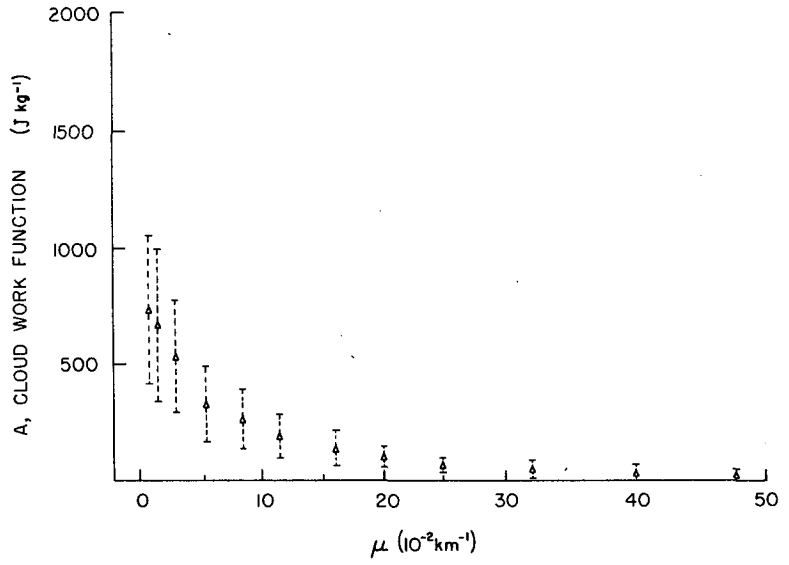


FIG. A2. As in Fig. 9 except that $\lambda = \mu$ is used as the spectral parameter.

entire range of each choice of spectral parameter even when the average relationship between the two parameters as shown in Fig. A1 is used. Fig. A1 shows that $\hat{p} = 200$ mb corresponds to $\mu = 0.016$ km$^{-1}$ on the average. The mean value of cloud-work function for the $\hat{p} = 200$ mb clouds in Fig. 9 is almost the same as the mean value for the $\mu = 0.016$ km$^{-1}$ clouds in Fig. A2. More importantly, the standard deviations of cloud-work function values are comparable between the two choices of parameter. This validates spectral decomposition of a cumulus ensemble into subensembles by either $\lambda = \mu$ or $\lambda = \hat{p}$.

## REFERENCES


Arakawa, A., and W. H. Schubert, 1974: Interaction of a cumulus cloud ensemble with the large-scale environment. Part I. *J. Atmos. Sci.* **31**, 674–701.

Charney, J. G., and A. Eliassen, 1964: On the growth of the hurricane depression. *J. Atmos. Sci.* **21**, 68–75.

Frank, W. M., 1977: The structure and energetics of the tropical cyclone I. Storm structure. *Mon. Wea. Rev.*, **105**, 1119–1135.

Jordan, C. L., 1958: Mean soundings for the West Indies area. *J. Meteor.*, **15**, 91–97.

Krishnamurti, T. N., 1969: An experiment in numerical prediction in equatorial latitudes. *Quart. J. Roy. Meteor. Soc.*, **95**, 594–620.

——, H. Pan, C. B. Chang, J. Ploshay, D. Walker and W. Oodaly, 1979: Numerical weather prediction for GATE. *Quart. J. Roy. Meteor. Soc.*, **105**, 979–1010.

Kuo, H. L., 1965: On the formation and intensification of tropical cyclones through latent heat release by cumulus convection. *J. Atmos. Sci.*, **22**, 40–63.

——, 1974: Further studies of the parameterization of the influence of cumulus convection on large-scale flow. *J. Atmos. Sci.*, **31**, 1232–1240.

Manabe, S., J. Smagorinsky and R. Strickler, 1965: Simulated climatology of a general circulation model with hydrological cycle. *Mon. Wea. Rev.*, **93**, 769–798.

Nitta, T., 1976: Large-scale heat and moisture budgets for the Air Mass Transformation Experiment. *J. Meteor. Soc. Japan*, **54**, 1–14.

Ooyama, K., 1964: A dynamical model for the study of tropical cyclone development. *Geofis. Int.*, **4**, 187–198.

——, 1971: A theory on parameterization of cumulus convection. *J. Meteor. Soc. Japan*, **49** (Special Issue), 744–756.

Thompson, R. M., Jr., S. W. Payne, E. E. Recker and R. J. Reed, 1979: Structure and properties of synoptic-scale wave disturbances in the intertropical convergence zone of the eastern Atlantic. *J. Atmos. Sci.*, **36**, 53–72.

Yanai, M., S. K. Esbensen and J.-H. Chu, 1973: Determination of bulk properties of tropical cloud clusters from large-scale heat and moisture budgets. *J. Atmos. Sci.*, **30**, 611–627.

——, J. H. Chu, T. E. Stark and Tsuyoshi Nitta, 1976: Response of deep and shallow tropical cumuli to large-scale processes. *J. Atmos. Sci.*, **33**, 976–991.